Chapter 4

Performance evaluation of tool coatings and nanofluid MQL on the micro-machinability of Ti-6Al-4V

The micromilling process has taken a prominent place in the micromachining industry due to its faster machining rate and applicability to a diverse range of engineering materials. However, this is especially troublesome for difficult-to-machine materials like Ti-6Al-4V alloy due to tool wear and catastrophic tool breakage, which are significant drawbacks that result in loss of surface quality. As a result, it is necessary to reduce the amount of burr generation, the surface roughness of microchannels, and catastrophic tool failure. In this study, it was tried to hybridize water and CuO nanofluid-based MQL with PVD-coated (AlTiN/TiAlN) and uncoated WC micro end-mills during the micromilling of Ti-6Al-4V alloy in order to improve the surface quality and prolong tool life. To assess the size, shape, and stability of nanofluids, CuO nanofluids were characterized using HR-SEM, XRD, zeta potential, and particle size analyser. Additionally, contact angle measurement has been used to examine the surface wettability of various coated and uncoated tools for combining various water-based CuO nanofluids.

4.1 Experimental procedure

4.1.1. Work material, coated tool, and MQL assisted micromilling

A 3-axis hybrid micro-machine (Model: DT-110, Manufacturer: Mikrotools Pte. Ltd.) with a positional accuracy of ± 1 μm and a maximum spindle speed of 60000 RPM was used for micro-milling of Ti-6Al-4V alloy, as shown in Fig. 4.1. An in-house fabricated MQL system was used for cooling and lubrication of the machining zone (Fig. 4.1). The MQL system contains an air compressor, pressure gauge, flow control device, and air atomizing nozzle (Spraytech Systems India Pvt. Ltd.). The gravity head

principle was adopted in this arrangement, where the coolant was supplied through gravity. A set of commercially available uncoated, AlTiN coated, and TiAlN coated tungsten carbide (WC) micro-mills (IND-SPHINX Precision Ltd.) is utilized to perform the full immersion micro-milling operations. Tool geometries and physical properties of uncoated, AlTiN coated, and TiAlN coated WC micro-mills are depicted in Table 4.1.

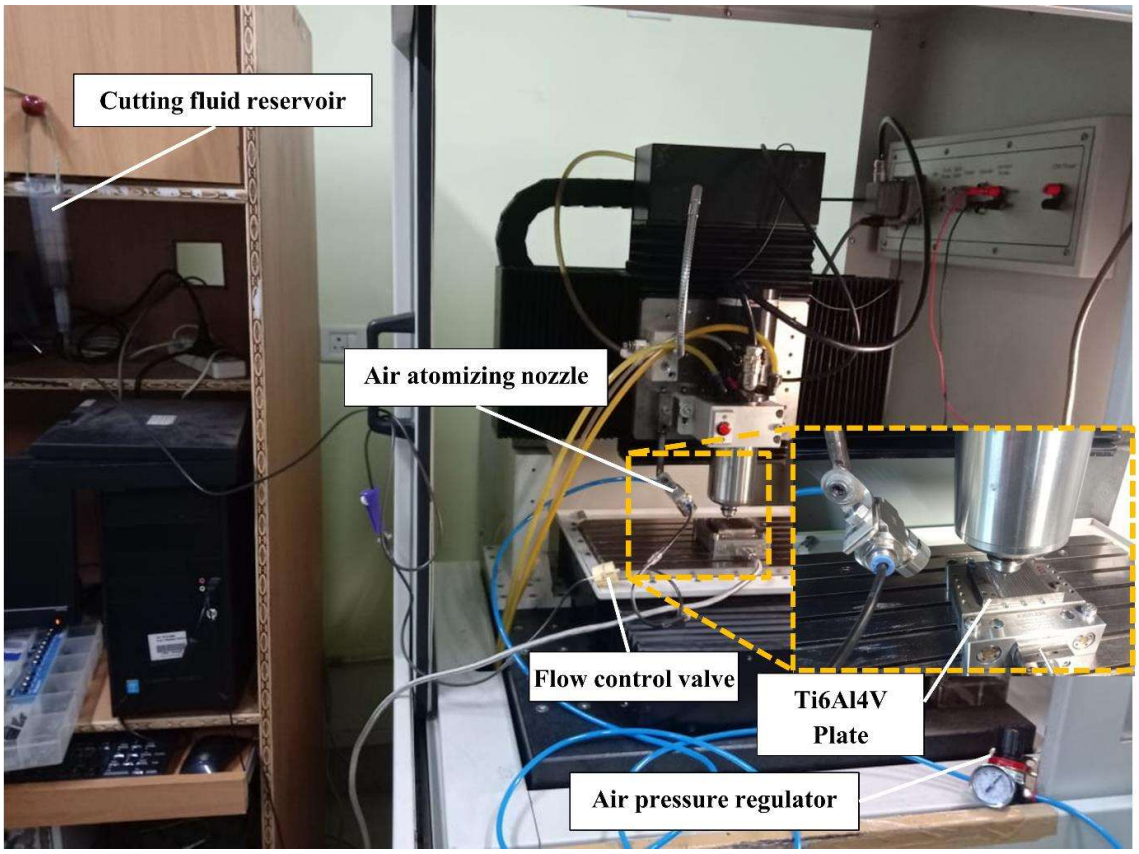

Fig. 4.1 DT 110 micromachine with MQL setup

Fig. 4.2 shows SEM images of the fresh TiAlN coated WC micro end-mill. Ti-6Al-4V grade 5 titanium alloy was used as the workpiece material in this study. Uncoated, AlTiN coated, and TiAlN coated WC micro-end mills, along with the different cutting environments such as dry, deionized water, 0.25 vol%, and 1 vol% of CuO water-based nanofluids, were used to machine the Ti-6Al-4V alloy plates of dimensions 55 × 45 × 5 mm^3. The microstructure and X-ray diffraction (XRD) of Ti-6Al-4V alloy as shown in

Fig. 4.3 (a, b), which consists of two phases, α, and β. Fig. 4.4 shows machined Ti-6Al-4V plates under different environmental conditions.

Table 4.1 Mechanical properties and geometry of uncoated, AlTiN, and TiAlN coated WC micro-mills

Property	**Tool Geometries**		
End-Mills	Uncoated WC	AlTiN coated WC	TiAlN coated WC
Nominal diameter (mm)	0.5	0.5	0.5
Number of flutes	2	2	2
Flute length (mm)	1	1	1
Overall length (mm)	38	38	38
Shank diameter (mm)	3	3	3
Coating thickness (µm)	-----	1	1
Cutting edge radius (µm)	1.536 to 1.852	2.134 to 2.756	1.984 to 2.657
Helix angle (°)	30	30	30
Microhardness (HV)	3200	3700	3500
Friction coefficient of WC ball against Ti6Al4V plate	0.5	0.38	0.4

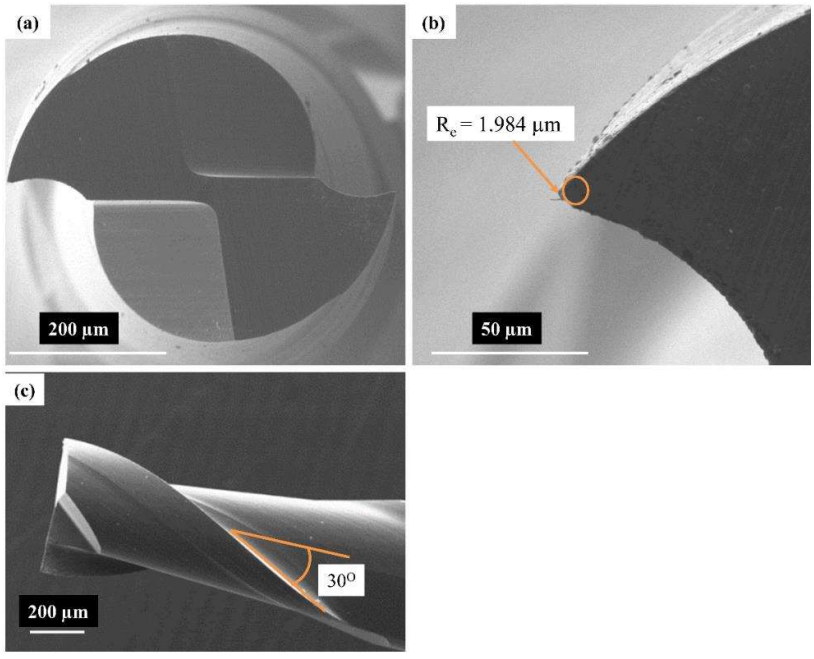

Fig. 4.2 SEM images of fresh TiAlN coated WC micro end-mill (a) bottom view, (b) cutting edge radius, (c) side view

Ten micro slots, each 45 mm in length, were generated with a fresh micro-mill under different experimental conditions. The spacing between consecutive slots is equal to the slot width (Fig. 4.5). The overhang length of the micro end-mill was 15 mm to avoid the tool run-out effects, which play a significant role in the micro-milling operation. Before performing the micromilling operation, the surface of the Ti-6Al-4V specimen was made flat by the grinding process. In order to maintain the uniform depth of cut, a skin cut was performed using a 3 mm end-mill. At constant machining parameters, such as a cutting speed of 47.12 m/min, feed rate of 240 mm/min, and depth of cut of 60 μm, ten slots of each 45 mm machining length were machined using TiAlN coated, AlTiN coated, and uncoated WC tools in various cutting environments. The micro-milling and MQL parameters utilized during the experiments, as shown in Table 4.2, were obtained by pilot tests. The combination of coated and uncoated WC tools and MQL conditions are listed in Table 4.3. Cutting forces were measured using a piezoelectric type mini dynamometer (Kistler, 9256C2) with an accessory of charge amplifier (Kistler 5070A) and data acquisition system (Kistler, 5697) by keeping the sampling frequency at 25 kHz.

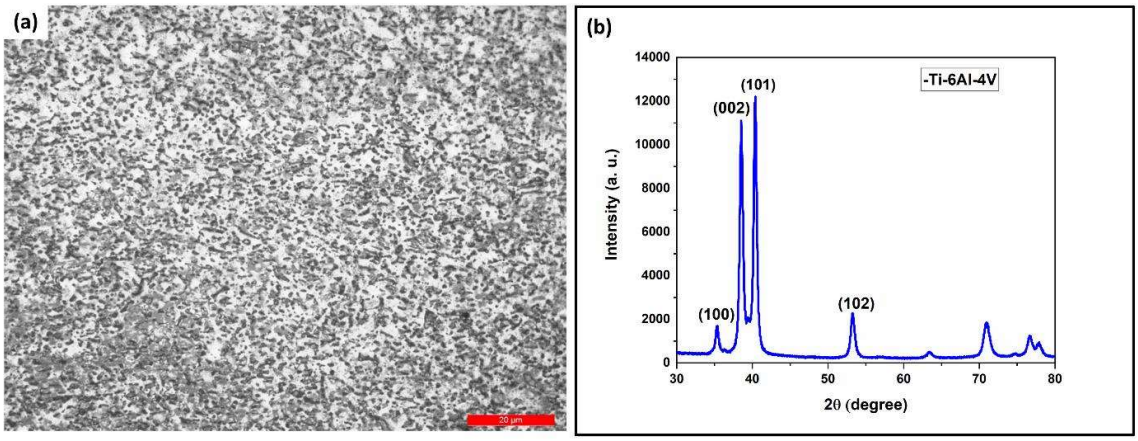

Fig. 4.3 (a) Microstructure and (b) XRD of Ti6Al4V alloy

The surface roughness of finished slots was measured using an optical profilometer (Taylor Hobson CCI) and a 5× lens with a scan area of 3.42 × 3.42 mm^2. The surface parameters of the microchannels were acquired using Talymap Gold software. The average surface roughness R_a was measured at the beginning, mid, and end of each microchannel along up milling, down milling, and centreline of the bottom of the microchannel. For each experimental condition, the surface roughness was measured at nine different locations on the bottom of the microchannel. The machined microchannels and burr formation in the 10^{th} microchannel of each condition were examined in up milling and down milling sides with the help of a scanning electron microscope (Zeiss EVO18 MA) at a magnification of 200×. Further, micro-channel burr width was measured by ImageJ1.52a software.

Table 4.2 Micro-milling parameters and MQL conditions

Process parameters	Units	Value
Spindle speed (N)	min^{-1}	30000
Feed rate (F)	mm/min	240
Radial depth of cut/ diameter of the tool	µm	500
Axial depth of cut	µm	60
Feed per tooth (f_z)	µm/tooth	4
Number of flutes	------	2
MQL flow rate	ml/h	50
Nozzle orifice diameter	mm	0.8
Air pressure	bar	3
The total length of cut per experiment	mm	450
Nozzle distance	mm	30
Nozzle angle	degree	45°

Table 4.3 Lubrication conditions with different coated tools

Run	Lubrication conditions	Type of tools used
1	Dry	Uncoated WC
2	Dry	AlTiN coated WC
3	Dry	TiAlN coated WC
4	Deionized water	Uncoated WC
5	Deionized water	AlTiN coated WC
6	Deionized water	TiAlN coated WC
7	0.25 vol% CuO nanofluid	Uncoated WC
8	0.25 vol% CuO nanofluid	AlTiN coated WC
9	0.25 vol% CuO nanofluid	TiAlN coated WC
10	1 vol% CuO nanofluid	Uncoated WC
11	1 vol% CuO nanofluid	AlTiN coated WC
12	1 vol% CuO nanofluid	TiAlN coated WC

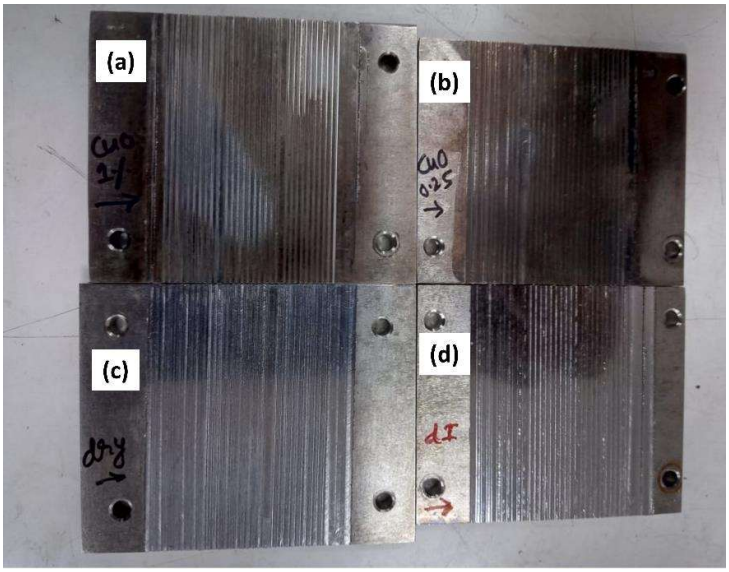

Fig. 4.4. Slots machined on Ti-grade 5 work material at (a) 1 vol% CuO nanofluid MQL condition, (b) 0.25 vol% CuO nanofluid MQL (c) dry and (d) pure MQL (deionized water)

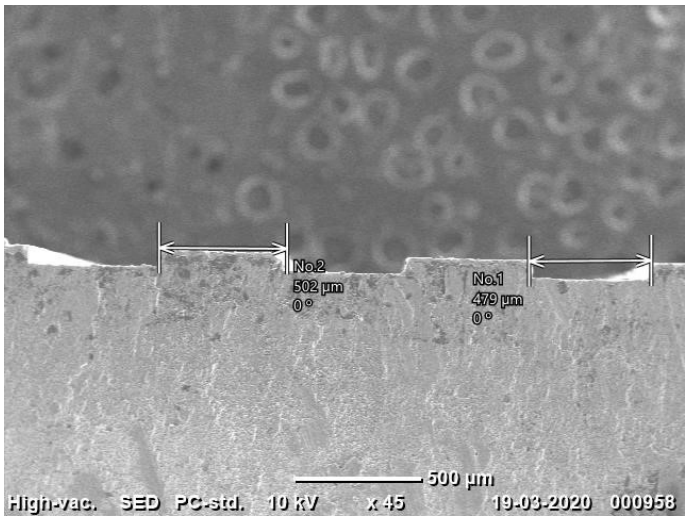

Fig. 4.5 Image of a cross-section showing space between two consecutive micro-grooves

4.1.2 Nano-cutting fluids: preparation and characterization

The HR-SEM image of CuO nanoparticles is shown in Fig. 4.6 (a), which indicates the spherical shape of nanoparticles. Nanoparticle size was determined by counting the number of particles in a predetermined area. It was found that the average size of spherical CuO nanoparticles is 24.74 nm (Fig. 4.6 (a, c)). Nanoparticles have been characterized using an XRD technique (Rigaku Miniflex 600 Desktop) to verify CuO particles. All peaks obtained in the XRD plot match with JSPDS 895897 card number (Fig. 4.6 (b)). For uniform dispersion, water-based CuO nanofluids were developed by a two-step method with a sodium dodecyl sulfate (SDS) surfactant. The volume concentrations of CuO nanoparticles in deionized water are 0.1, 0.25, 0.5, 0.75, and 1 vol%. The density of CuO nanoparticles and deionized water is 6.4 g/cc and 1 g/cc. The relation between the weight of nanoparticles and vol% of nanoparticles is shown by Eq. (4.1). The quantity of SDS is $1/10^{th}$ weight of CuO nanoparticles. The volume concentration of nanoparticles is calculated as follows:

$$\% \text{ volume concentration of nanoparticles} = \frac{\left(\frac{W_{CuO}}{\rho_{CuO}}\right)}{\left(\frac{W_{CuO}}{\rho_{CuO}}+\frac{W_{bf}}{\rho_{bf}}\right)} \times 100\ \% \quad (4.1)$$

where, $W_{cuo,}$ *and* W_{bf} = Weight of CuO nanoparticles and base fluid

ρ_{cuo} *and* ρ_{bf} = Density of CuO nanoparticles and base fluid

For uniform dispersion of nanoparticles in the deionized water, firstly test sample was mixed through a magnetic stirrer for 2 h. Further, these samples were kept in the ultrasonication bath for 1 h. Nanofluids stability is crucial for adequate lubrication, mainly upset by the aggregation of nanoparticles caused by Vander Waal forces. Zeta potential method has been used to precisely evaluate the stability of the nanofluids. A higher zeta potential value indicates more stabilized nanofluids. Dynamic light scattering (DLS) estimates the hydrodynamic diameter of spherical nanoparticles within the dispersion. The particle size is determined by arbitrary changes in light intensity from a monochromatic laser source scattered passing through the suspension. Stoke-Einstein equation converts the diffusion of the nanoparticles driving under Brownian motion to particle size. The stability of particles in nanofluids was measured by zeta potential analysis and DLS test on the Malvern zeta sizer nano series. The absolute zeta potential value of CuO nanofluids at %volume concentrations 0.1, 0.25 and 0.5, and 0.75 are -23.37 mV, -24.97 mV, -37.61 mV, and -24.65 mV, respectively (Fig. 4.7). The average aggregate size of CuO nanoparticles dispersed in deionized water with 0.1, 0.25, 0.5, and 0.75 vol% was 301 nm, 165.6 nm, 192.7 nm, and 260.5 nm, as shown in Fig. 4.8.

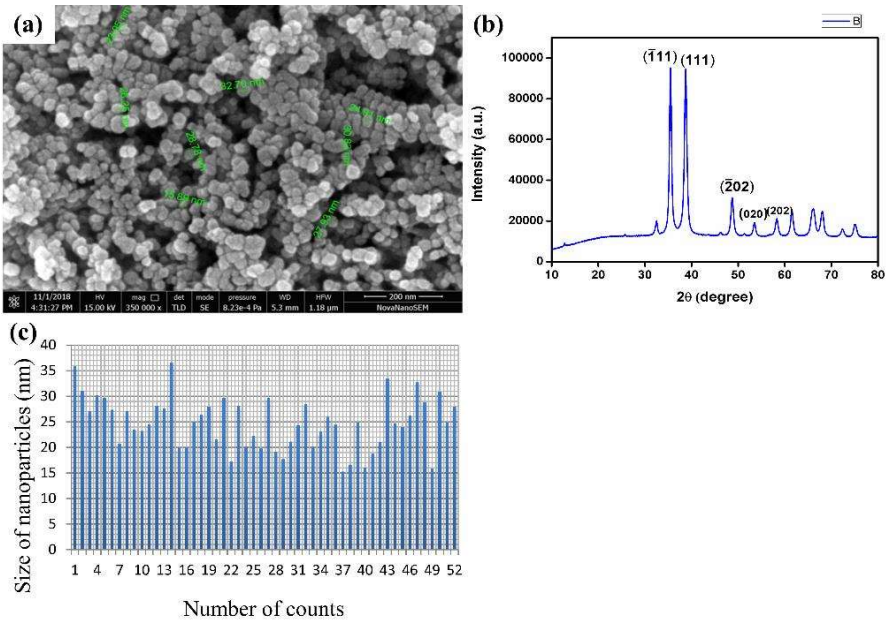

Fig. 4.6 (a) SEM image of CuO nanoparticles (b) XRD of CuO nanoparticles (c) size of nanoparticles versus the number of counts

Beyond 0.75 vol%, it is difficult to determine the average aggregate size of CuO nanoparticles in dispersion due to their dark black colour and the inability to scatter light through dispersion. Dynamic viscosity of deionized water-based CuO nanofluids is measured at 0, 0.1, 0.25, 0.5, 0.75, and 1 vol% on Brookfield Viscometer, and corresponding values are 0.89 cP, 0.97 cP, 0.99 cP, 1.01 cP, 1.02 cP, and 1.04 cP respectively. It is found that viscosity increases with an increase in the concentration of CuO nanoparticles. There was an increase of 16.85% at 1 vol% CuO nanofluids compared to deionized water. Due to the high viscosity of 1 vol% CuO nanofluids, nanodroplets stick to the tool-workpiece interface for a larger time than pure MQL, show better lubrication, and reduce the friction as well between chip and tool. Besides, CuO has excellent heat transfer capacity, which helps to minimize the machining temperature and tool wear rate.

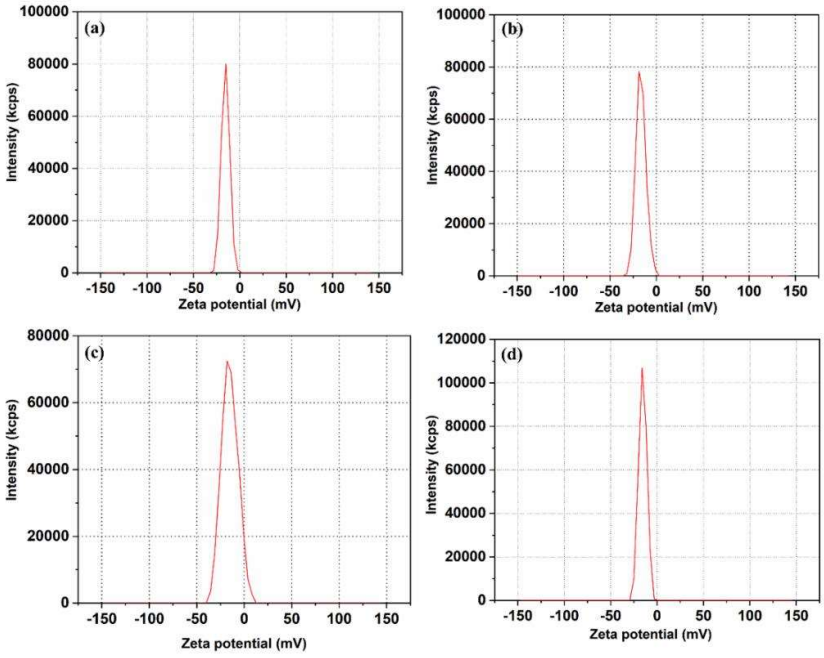

Fig. 4.7 Zeta potential of CuO nanofluids at (a) 0.1 vol% (b) 0.25 vol% (c) 0.5 vol% (d) 0.75 vol% concentration

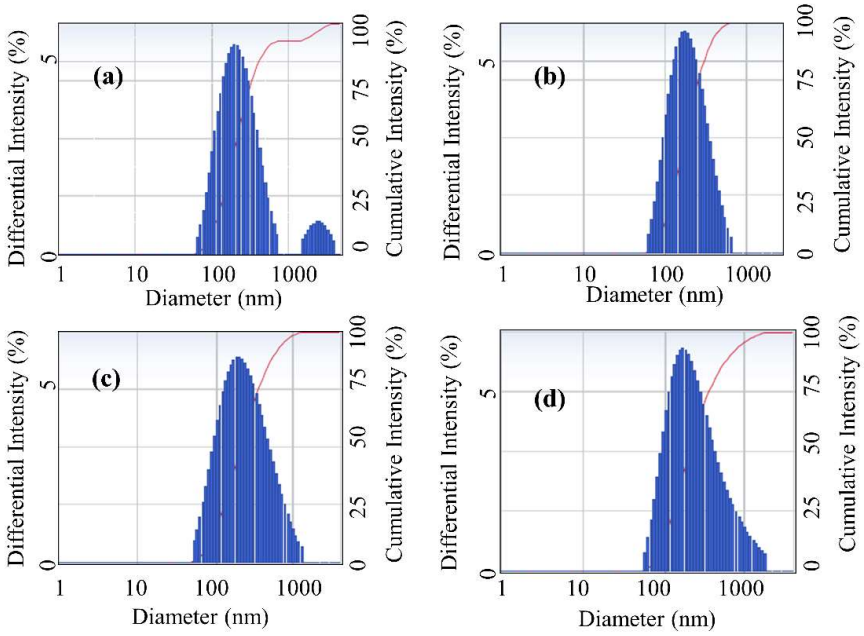

Fig. 4.8 Size distribution of aggregated CuO nanoparticles in deionized water at (a) 0.1 vol% (b) 0.25 vol% (c) 0.5 vol% (d) 0.75 vol% concentration

4.1.3 Wettability analysis

Wettability depicts the spreading of lubricant over the tool surface and enhances heat transfer in a larger area. The macroscopic contact angle results from the combined effect of adhesive and cohesive forces operating on the interface region. The minimum Helmholtz free energy is achieved by spreading the liquid droplet, resulting in the specification of the equilibrium contact angle. The free energy relies on the potentials of constituent molecules and atoms, mainly Vander Waal force, which also affects surface tension. These forces interplay on a nanometer range, which is comparable to the size of nanoparticles. As a result, adding nanoparticles to a pure liquid-solid-air contact is expected to impact the gross free energy [96]. Young's equation depicts the relation between equilibrium contact angle and surface tension of different phases (Fig. 4.9 (a)).

$$\mathrm{Cos}\Theta_e = \frac{\gamma_{sv} - \gamma_{sl}}{\gamma_{lv}} \tag{4.2}$$

where γ_{sv}, γ_{sl}, and γ_{lv} are denoted as interfacial surface tension among solid-vapor, solid-liquid, and liquid-vapor states.

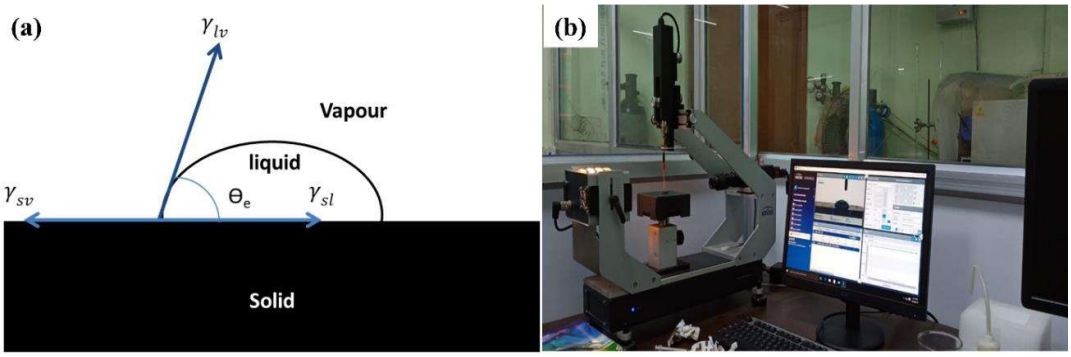

Fig. 4.9 (a) Wettability of nanofluids droplet on the solid substrate (b) pictorial view of contact angle measurement setup

A drop shape analyzer 25 (Manufacturer: KRUSS) was used to assess the contact angle for all lubricant samples on uncoated and coated surfaces at different

nanoparticle concentrations ranging from 0% to 1%, as shown in Fig. 4.9 (b). The sessile drop technique was utilized to analyze the wettability of the lubricants. The substrates were cleaned with acetone before conducting the wettability test. Droplets of deionized water and water-based CuO nanofluids with a known volume of 2 μL were deposited using a syringe attached to the spring on AlTiN coated, TiAlN coated, and uncoated WC substrates at ambient temperature. For all lubricant samples (at various nanoparticles concentrations from 0% to 1%), contact angles were measured on the uncoated, TiAlN coated, and AlTiN coated WC surface (Fig. 4.10). Fig. 4.10 (a) and (b) illustrate the hydrophobic nature of deionized water and 0.1 vol% CuO nanofluids with uncoated WC substrate. Fig. 4.10 (c–f) shows the improvement of wettability on uncoated WC substrate with an increase in the concentration of nanoparticles. The contact angle on AlTiN coated surface is shown to decrease as the nanoparticle concentration increases from 0% to 1% (Fig. 4.10 (m–r)). A similar observation was also indicated on the TiAlN coated surface (Fig. 4.10 (g–l)). These results show that the contact angle decreases with an increase in the volumetric concentrations of nanofluids due to structural disjoining pressure, which is responsible for the spreading of nanofluids [97, 98]. If the viscosity factor dominates over structural disjoining pressure, the contact angle increases with increased volume concentration. It may be confirmed by the results of Sharma et al. [99]; they observed an improvement in the wettability of nanofluids with an increase in nanoparticles concentration from 0.25 vol%–1 vol%. Beyond 1 vol% concentration, the contact angle increased.

4.2 Results and discussion

4.2.1 Tool wear

Tool wear standard ISO-8688-2 for conventional machining is not applicable to micromilling due to different wear characteristics. In this work, the main attention is to

analyze the tool wear and wear mechanism related to the micromilling of Ti-6Al-4V alloy using uncoated and coated WC tools under different cutting environments. After 450 mm machining length, tool wear was analyzed by scanning electron microscope (SEM) images and energy-dispersive X-ray spectroscopy (EDS). From the SEM images and EDS analysis, as shown in figures (Figs. 4.11-4.17), tool wear was observed mainly in the form of adhesion, abrasion, grains pull-out, edge chipping, built-up edge, and coating delamination.

Fig. 4.11 shows the SEM micrograph of the worn uncoated, and coated (TiAlN and AlTiN) WC tools in dry condition. As shown in Fig. 4.11(a) and (b), edge chipping was observed in the case of uncoated and TiAlN coated WC tools. This tool wear occurs due to the combined influence of residual stress, cyclic loading, and abrasion [100, 101]. Due to severe interaction between the cutting tool and workpiece, abrasion wear occurs, and the edge radius of the tool increases. Due to the increase of edge radius, effective stress rises on the cutting tool, and higher cutting temperature develops in the cutting zone [102]. Further, Peng et al. [101] reported that a higher tool edge radius and negative rake angle increase residual stress, which results in chipping and breakage of the cutting edges. Fig. 4.11 (c) shows the SEM image of the worn AlTiN coated WC tool under dry conditions. It indicates that adhesion wear and coating delamination were predominant on one of the edges of the micro end-mill. From the EDS analysis depicted in Fig. 4.11 (d), the presence of W and C elements on the tool surface confirms the coating delamination. Further, significant adhesion has been observed on the flank surface of the tool. Further, it has been noted that delamination occurs due to a fracture spreading at the coating as a consequence of the difference in the coefficient of thermal expansion between the coating layer and substrate material [103].

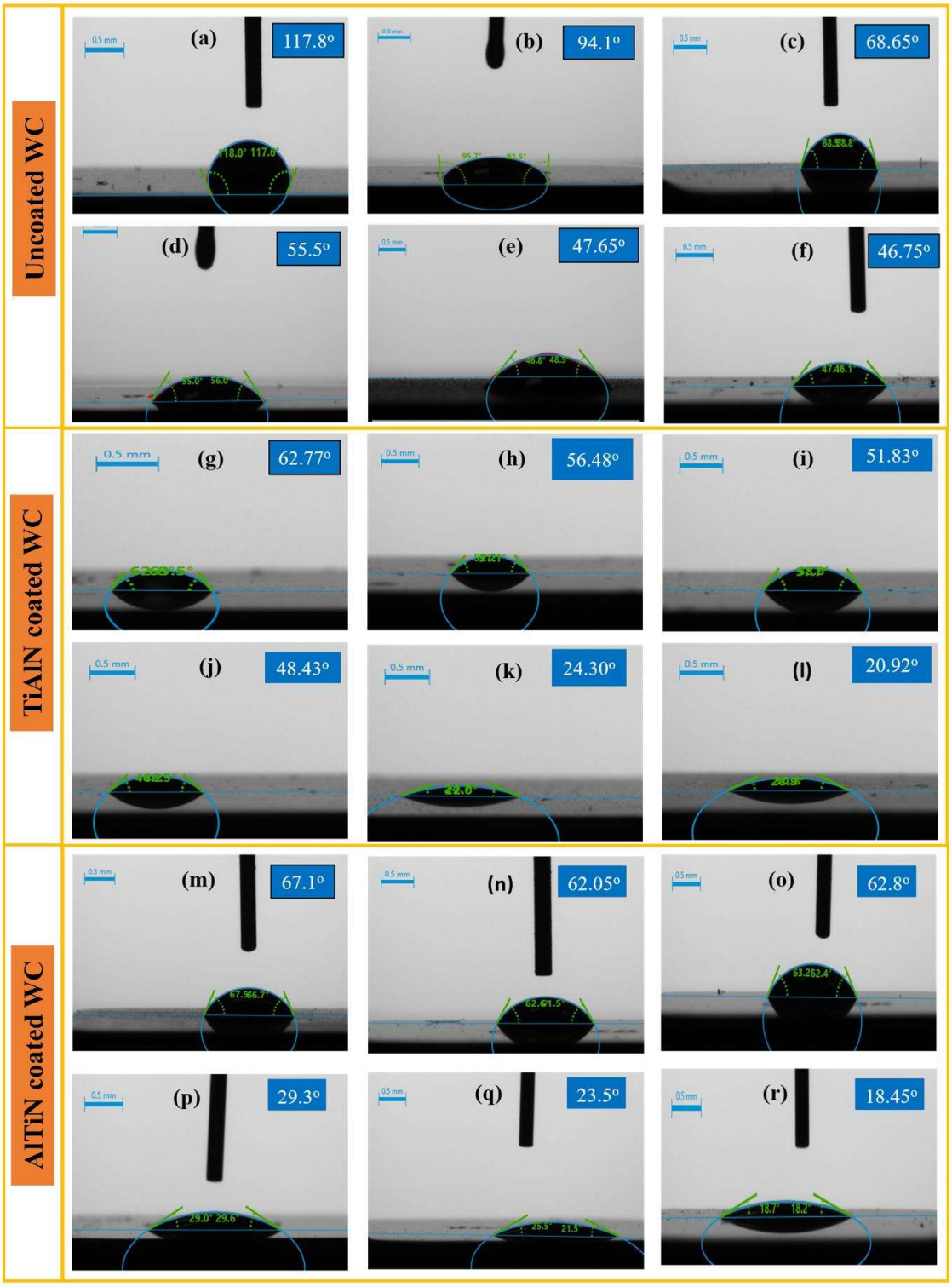

Fig. 4.10 Examples of drop pendants of deionized water and CuO nanofluids on uncoated surface at (a) 0 vol% (b) 0.1 vol% (c) 0.25 vol% (d) 0.5 vol% (e) 0.75 vol%

(f) 1 vol%, TiAlN coated surface at (g) 0 vol% (h) 0.1 vol% (i) 0.25 vol% (j) 0.5 vol% (k) 0.75 vol% (l) 1 vol% and AlTiN coated surface at (m) 0 vol% (n) 0.1 vol% (o) 0.25 vol% (p) 0.5 vol% (q) 0.75 vol% (r) 1 vol%

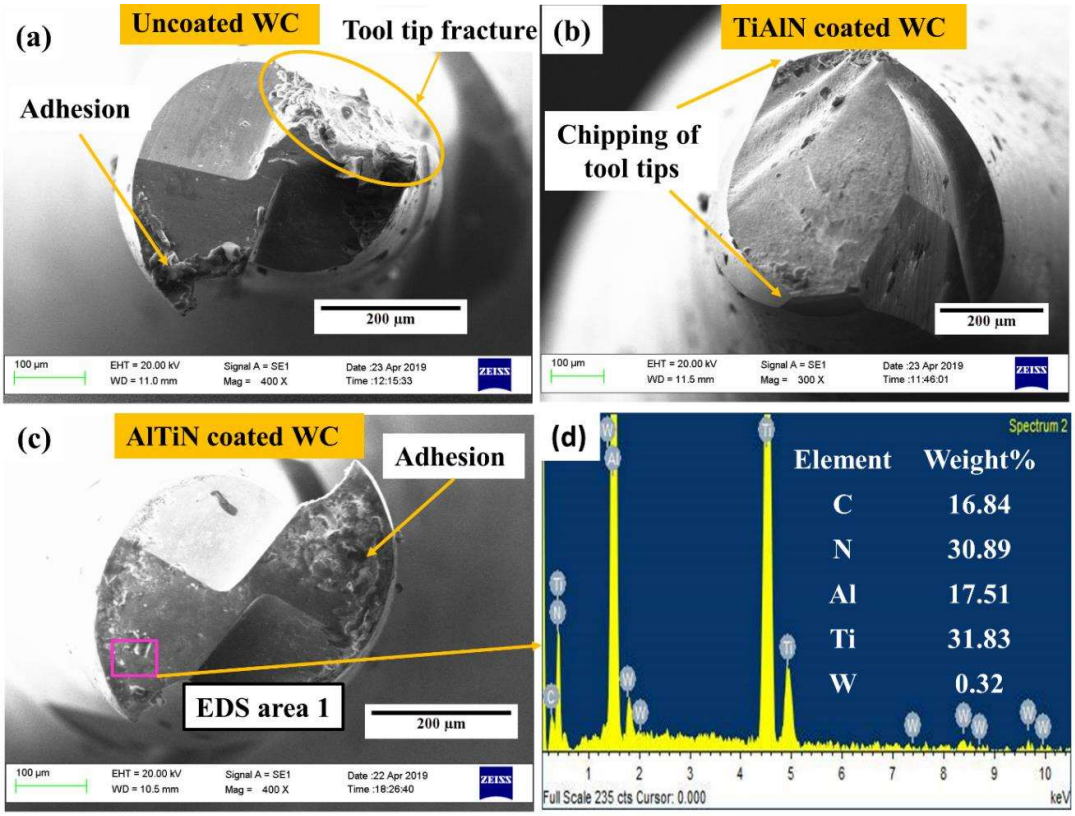

Fig. 4.11 SEM images of (a) uncoated, (b) TiAlN coated, and (c) AlTiN coated WC micro mills in dry condition with (d) EDS analysis of AlTiN coated cutting edge after cutting process of 450 mm length

As the AlTiN/TiAlN coating delamination begins, a chemical affinity between Ti6Al4V and WC/Co begins, which promotes Ti6Al4V adhesion at the tool edge. Edge chipping or flaking occurs when certain tool segments have been removed along with the adhesive layer of work material. Chipping and/or flaking of the tool material are results of the cyclical formation and detachment of the adhesive layer [104].

In the present study, adhesion wear was found to be more pronounced than abrasion wear in respective cutting environments due to the higher hardness and lower

frictional coefficient of the AlTiN coated WC tool. High pressure and temperature generated between the chip and the rake face produce a suitable environment for chip adherence to the tool surface. Fig. 4.12 shows the SEM micrographs of the worn tools in pure MQL conditions. For the uncoated WC micro-mill, as shown in Fig. 4.12 (a), tool wear was observed in the form of built-up edge formation and edge chipping of the tool. Built-up edge formation and coating delamination were observed as significant tool wear phenomena, as shown in Fig. 4.12 (b, c) for the coated tools. The WC substrate was revealed after removing the coating using a mixture of abrasion, attrition, and spalling. This appears to be caused by the coating's inherent residual stress and the localized mechanical stresses imparted on the coating by the end mill's intermittent contact throughout high-speed micromilling. The beginning of the micro-crack commences under the influence of cyclic stresses. Subsequently, these micro-cracks spread, leading to cutting edge chipping [105]. The EDS analysis, as shown in Fig. 4.13 (a), confirms the adhesion of the workpiece material on the tool surface as significant weight % of Al (32.49%) and Ti (58.35%) were found on the uncoated tool surface. From the EDS analysis, as shown in Fig. 4.13 (b, c), W and C were found on the flank face, which is the base material of the cutting tool. Tool wear in the form of adhesion and chipping was found to be less in coated tools than in uncoated ones. This is due to the combined influence of hard coating and lubrication.

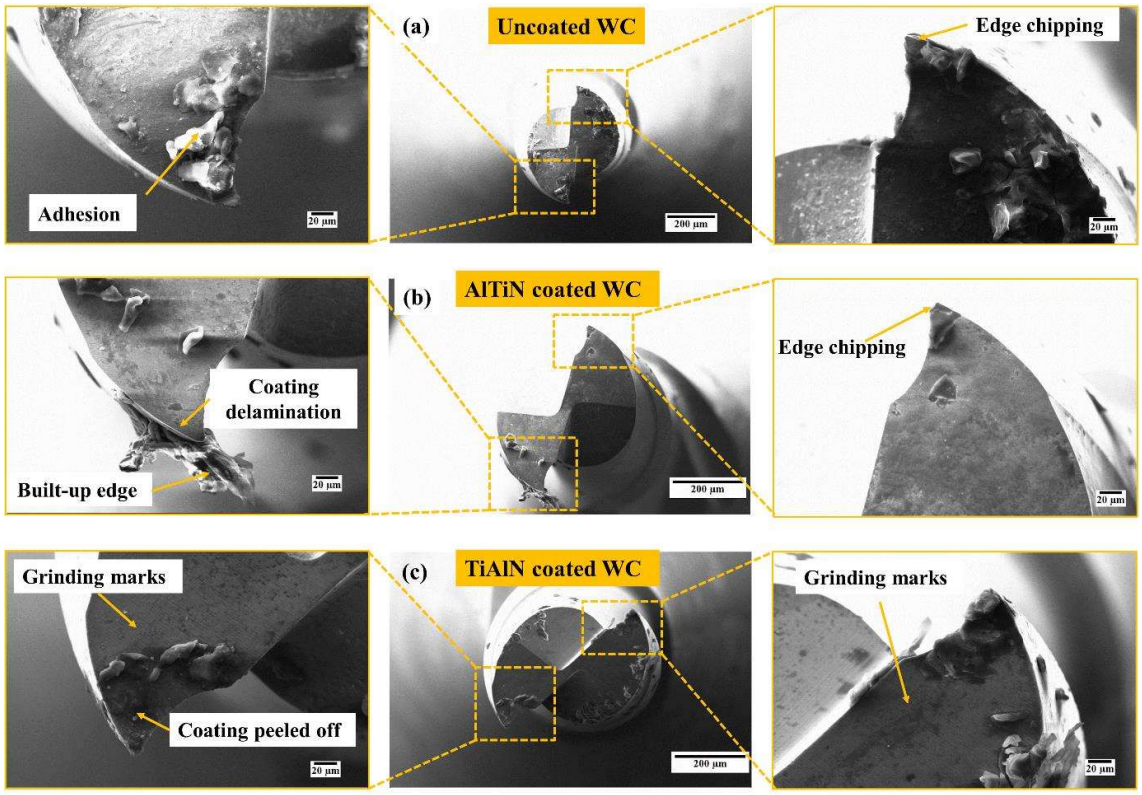

Fig. 4.12 SEM images of (a) uncoated, (b) AlTiN coated, and (c) TiAlN coated WC micro end-mills with an enlarged view of both cutting edges in pure MQL condition (deionized water) after 450 mm cutting length

In subsection 4.1.3 (refer to Fig. 4.10 (a, g, m)), it was observed that coated surfaces behave hydrophilic with deionized water, whereas the uncoated surface behaves hydrophobic nature. Therefore, the hydrophilic nature of the coated tools favours the contact of the lubrication with the tool surface during machining and reduces heat generation [106]. As a result, adhesion of the workpiece material and the chipping of the edges were observed less in the case of coated tools.

The surface morphologies of uncoated and coated tools under 0.25 vol% CuO NF-MQL conditions are shown in Fig. 4.14. Cutting edge rounding and edge chipping were observed in the case of the uncoated WC tool, as shown in Fig. 4.14 (a). However, in

the case of coated tools, as given in Fig. 4.14 (b, c), the cutting edges were intact, with good sharpness and coating delamination on the tool flank face. Flank wear and material adhesion were observed on TiAlN coated tool, as shown in Fig. 4.14 (c). Fig. 4.15 shows the surface wear morphologies and EDS micrographs of uncoated, AlTiN, and TiAlN coated WC micro end-mills after a cutting length of 450 mm. The energy spectrum of the coated tools depicts partial delamination of coating from the tool surface as the weight % of W and C was less.

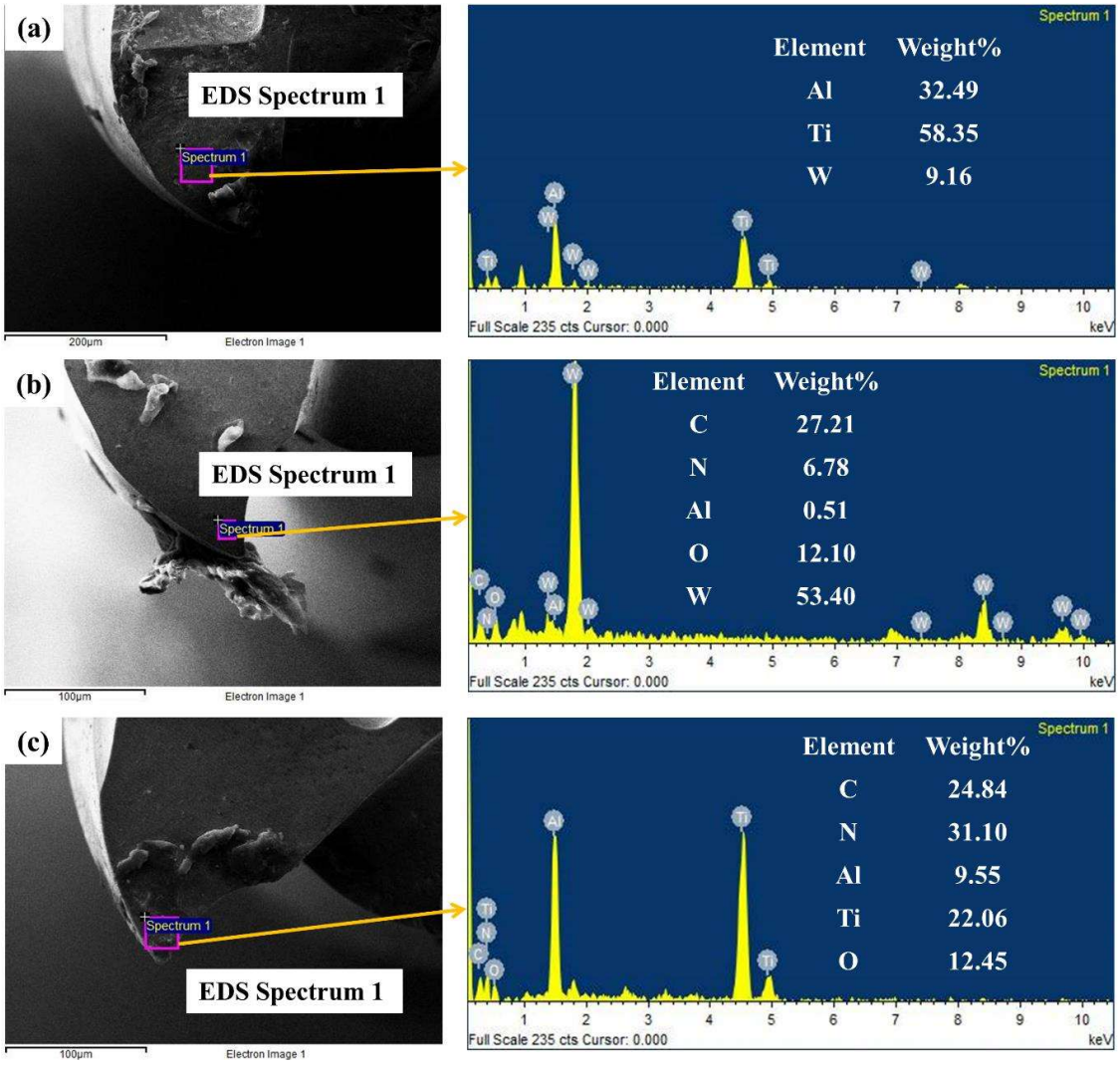

Fig. 4.13 EDS results of (a) uncoated, (b) AlTiN coated, and (c) TiAlN coated WC micro end-mills in pure MQL condition after 450 mm cutting length

CuO nanoparticles efficiently prevented chips from adhering to the micro-mill because its ball-bearing effect was a key factor here. When compared to pure water, adding 0.25 vol% CuO nanoparticles to deionized water improves its wettability significantly. Enhancement of wetting area per unit volume improves lubrication and heat removal capabilities.

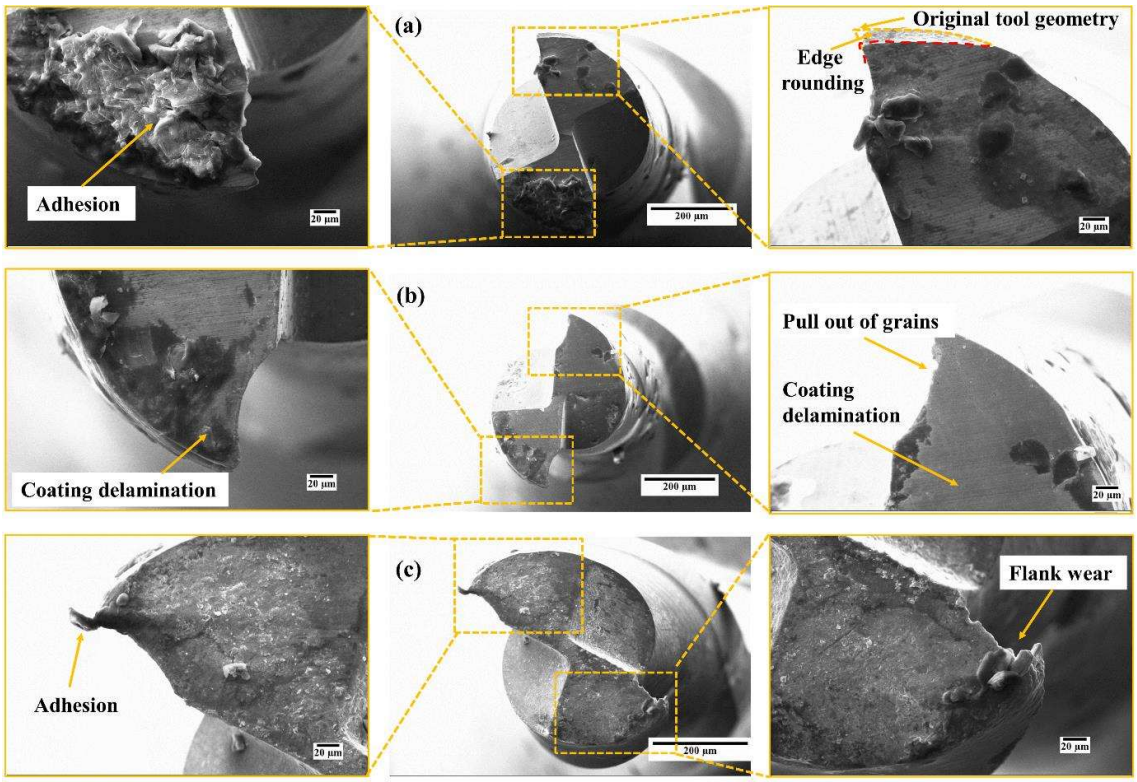

Fig. 4.14 SEM images of (a) uncoated, (b) AlTiN coated, and (c) TiAlN coated WC micro mills in nanofluid MQL condition with 0.25 vol% CuO after 450 mm cutting length

The surface morphologies of uncoated, AlTiN coated, and TiAlN coated WC tools with an enlarged view of both cutting edges after machining utilized in 1 vol% CuO nanofluids MQL condition are shown in Fig. 4.16. Fig. 4.16 (a) shows the absence of built-up edge and material adhesion on the uncoated WC micro end-mill. This happens due to the enhanced lubrication and cooling rate of nanofluids with an

increased volume percentage of CuO nanoparticles. There was no microchipping, tool fracture, or abrasive wear on the cutting edges after machining 450 mm. A similar observation occurred in the AlTiN coated WC micro end-mill shown in Fig. 4.16 (b). In Fig. 4.16 (c), edge rounding on one edge of the micro end-mill and no adhesion and built-up edge formation were observed on the cutting tool. It means that with the increase in nanoparticle concentration, the thermal conductivity of nanofluids increases, resulting in more heat dissipation from the tool and preventing adhesive wear or built-up edge formation [107]. Similar outcomes were obtained by Rabie et al. [108] when 2.5 wt% CuO nanoparticles were added to water to form nanofluids and used in MQL-assisted grinding of 52100 hardened steel. They found a 15.9% reduction in grinding temperature using CuO nanofluid MQL compared to dry conditions. Huang et al. [109] compared the variations in the micromilling temperature when micro-milling SKH-9 high-speed steel at various weight percentages of graphene. Micromilling temperature (65.87 °C) was shown to be most affected or reduced by higher nanofluid density (1.0 wt%). They measured micromilling temperatures for water based MQL as a base fluid, MWCNT based NFMQL, and graphene based NFMQL and found average micromilling temperatures of 78.97, 71.3, and 69.05 ^{o}C. Further, they found that utilization of nanofluids at 1 wt% reduces tool wear. In contrast, Chu et al. [110] discovered that when micromachining 12L14 steel, 0.1 wt% and 0.2 wt% of ultrasonically and thermally exfoliated graphene oxide platelets showed maximum temperature reductions of 51% and 43%, respectively, compared to base fluid. Despite the fact that thermal conductivity rises as nanoplatelet weight percentage increases.

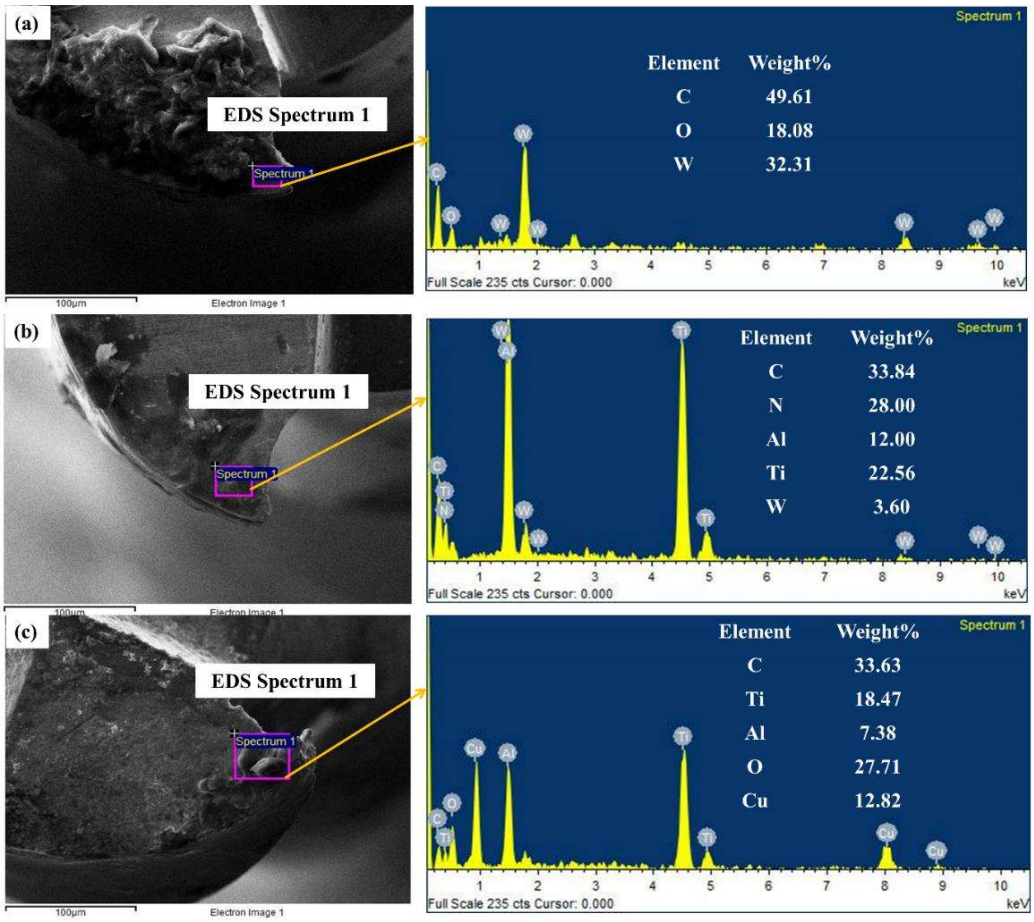

Fig. 4.15 EDS results of (a) uncoated, (b) AlTiN coated, and (c) TiAlN coated WC micro end-mills in 0.25 vol% CuO nano-MQL condition after 450 mm cutting length

The energy spectrum of the uncoated WC tool also indicates the absence of chip constituents on it (Fig. 4.17 (a)). The high weight percentage of Al and Ti elements in the TiAlN coating shows the absence of coating delamination (Fig. 4.17 (b)). From the comparative analysis of different cutting environments, it is found that 1 vol% CuO NF-MQL with uncoated WC tool shows better results for reduction of tool wear, adhesive wear, coating delamination, and edge chipping. Tool wear was reduced considerably in the case of nano-cutting fluids due to their superior conduction, convection, and spreadability compared to deionized water. It is constrained to the cutting edge portion only [111]. The tool possesses sharpness for an extended period of time due to the

enhanced cooling and lubricating qualities of nano-cutting fluids. As a result, adhesion wear is minor in 1 vol% CuO nanofluid compared to other lubricating conditions.

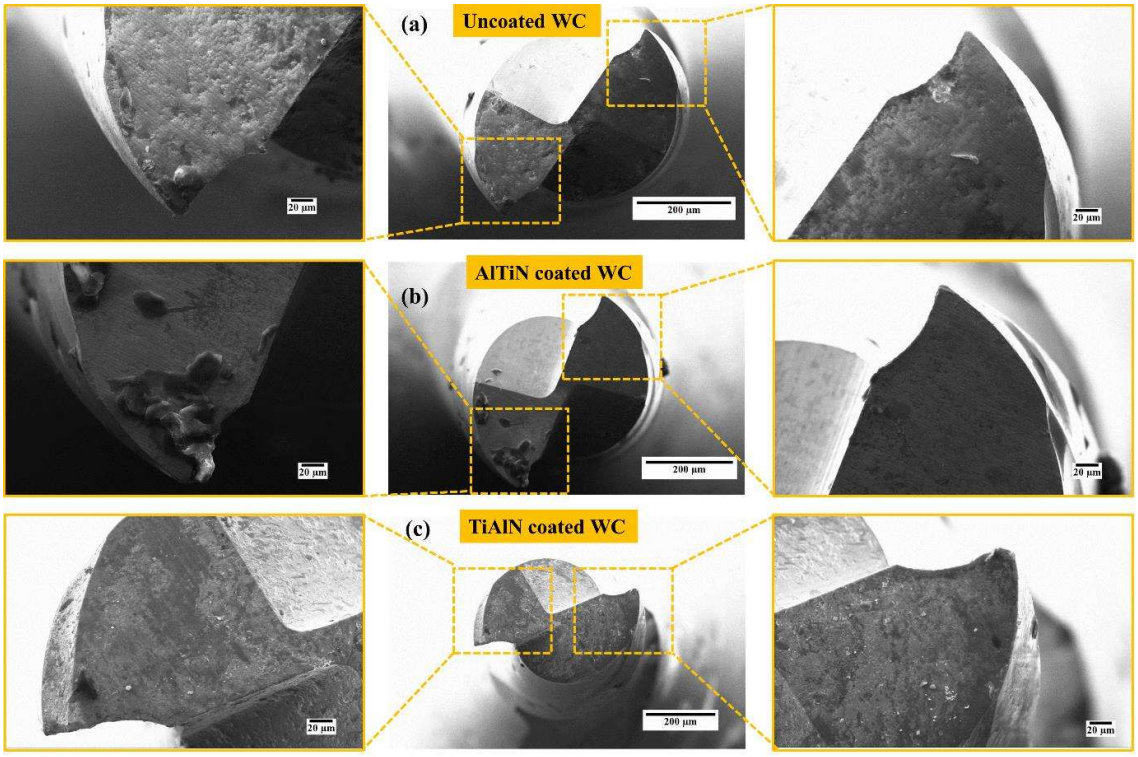

Fig. 4.16 SEM images of (a) uncoated, (b) AlTiN coated, and (c) TiAlN coated WC micro end-mills in nano-MQL condition with 1 vol% CuO after 450 mm cutting length

Fig. 4.18 shows the percentage diameter reduction of the micro-mill used to machine 450 mm under different cutting environments. Percentage tool diameter reduction was obtained by measuring the initial tool diameter of the new tool and tool diameter after machining a length of 450 mm for each condition. TiAlN coated tool in Pure MQL condition shows the least value of tool diameter reduction, and in dry condition, it depicts the worst result. Although uncoated WC tool in 1 vol% CuO NF-MQL condition also shows lower tool diameter reduction. This can be demonstrated by the fact that 1 vol% nanofluids form a thin lubricant film in the tool flank surface and tool-workpiece interface, which reduces friction and dissipates higher heat.

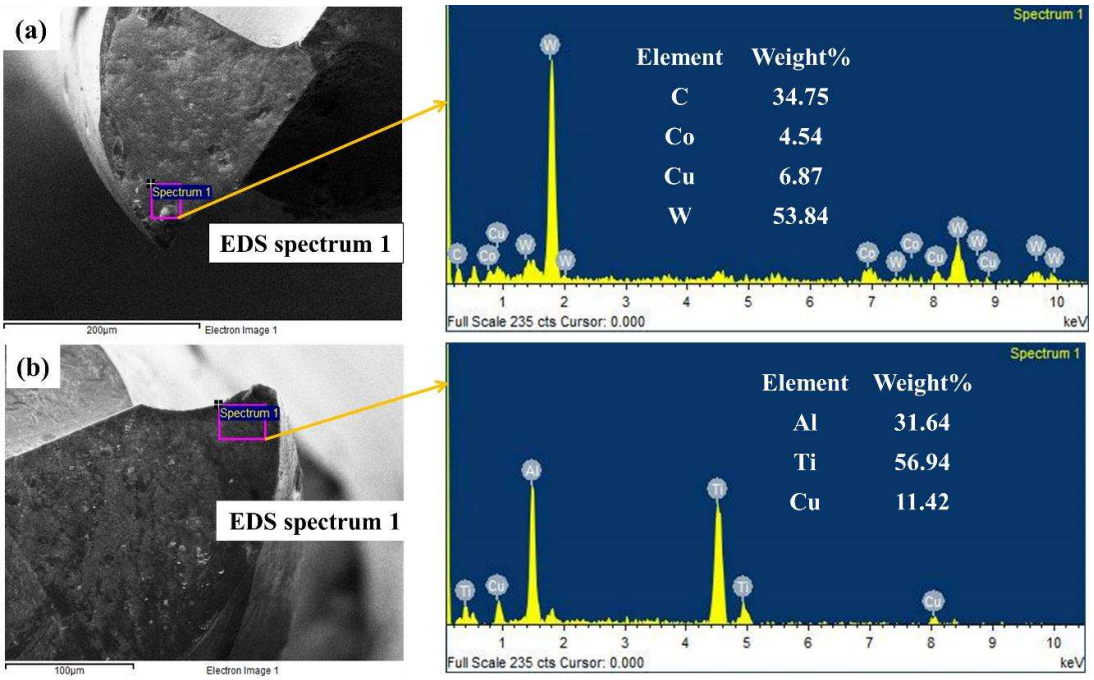

Fig. 4.17 EDS results of (a) uncoated and (b) TiAlN coated WC micro end-mills in 1 vol% CuO nano-MQL condition after 450 mm cutting length

Lubricant film protects the coating from delamination and increases tool life. Due to the small size of nanoparticles, which can easily penetrate the interface zone and act as a third body to protect the tool from abrasion. It was suggested that a lower contact angle enhances the capacity of nanofluids to spread and maintain interaction with surfaces, allowing for increased cooling/lubrication through the vaporization of the tiny droplets [96].

4.2.2 Cutting forces

Peak-to-valley forces are preferred for mean forces because they accurately represent lubrication related changes when computed at 100 tool rotations. After that, the machining length was plotted with the average peak-to-valley forces to observe the machining condition.

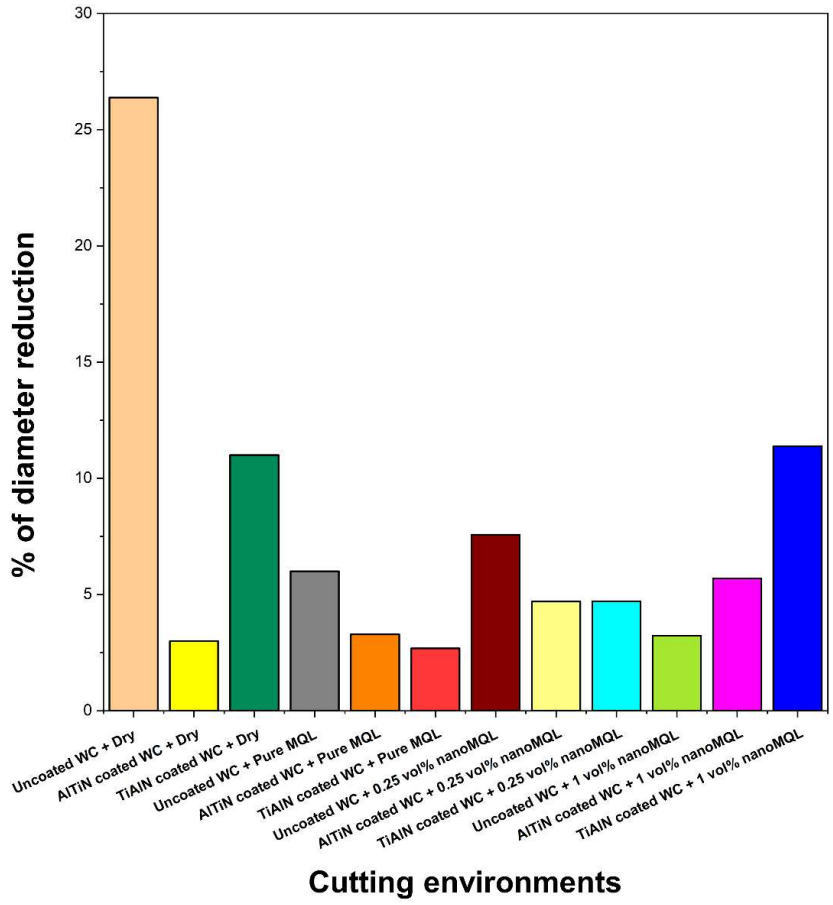

Fig. 4.18 Tool diameter reduction (%) with different cutting environments after 450 mm machining length

Feed force (F_x) refers to the force applied along the milling cutter's feed path, while cross-feed force (F_y) refers to the force applied perpendicular to the feed direction. Using the following equation, the resultant cutting force was determined as follows:

$$F = \sqrt{F_x^2 + F_y^2} \tag{4.1}$$

Using uncoated, AlTiN coated, and TiAlN coated WC micro-mills, Fig. 4.19 shows the cutting forces observed in micromilling using dry, deionized water MQL, 0.25 vol%

CuO nanofluid MQL, and 1 vol% CuO nanofluid MQL conditions. In dry conditions, the deterioration of tool geometry leads to increased cutting forces for uncoated and TiAlN coated WC micro mills. The tool chipping produced during the following machining operation accelerates the tool edge radius. In an uncoated WC micro-mill, the cutting force is lower than 1.25 N up to 360 mm of cutting distance. Cutting force dramatically increases after 360 mm of cutting length. Higher fatigue stress due to repetitive loads under dry conditions in an uncoated WC micro-mill causes one of the cutting edges substantial deteriorations and rapidly increases the magnitude of cutting force (Figs. 4.11(a) and 4.19). In contrast, AlTiN coated tool shows the minimum value of cutting force due to its higher hardness and wear resistance. The cutting force with coated WC micro-mills in deionized water conditions is significantly lower than that of an uncoated WC micro-mill in dry and MQL conditions. It shows increasing trends in cutting force, with cutting lengths going above 1.25 N for dry conditions. According to Fig. 4.19, machining under nanofluid MQL conditions with 0.25 vol% and 1 vol% CuO nanoparticles results in a lower cutting force than in dry and pure MQL settings. Because of their spherical shape, CuO nanoparticles create a nano ball-bearing effect between the surface layer, translating sliding friction into rolling friction and lowering friction. The increase in the load-bearing capability of nanofluids owing to the presence of nanoparticles is another reason for cutting forces reduction. The lowest resultant cutting forces are observed below 0.4 N in 0.25 vol% CuO nanofluid MQL conditions with AlTiN coated WC micro-mill. Despite nanoparticles' efficiency being limited by their concentration, abundant nanoparticles in the cutting region negatively influence the space for rolling and ductility, resulting in raised micromilling force. Hence lower concentrations of CuO nanoparticles resulting lower cutting forces than higher concentrations. AlTiN coated and TiAlN coated tools both exhibit an analogous

variation in cutting forces with machine length (Fig. 4.19). As a result, Fig. 4.20 shows the profile of cutting force generation with cutting time or revolutions for AlTiN coated and uncoated WC tools. In Fig. 4.20 for the uncoated and AlTiN coated WC micro-mill, measured feed forces illustrate the typical nature of cutting forces.

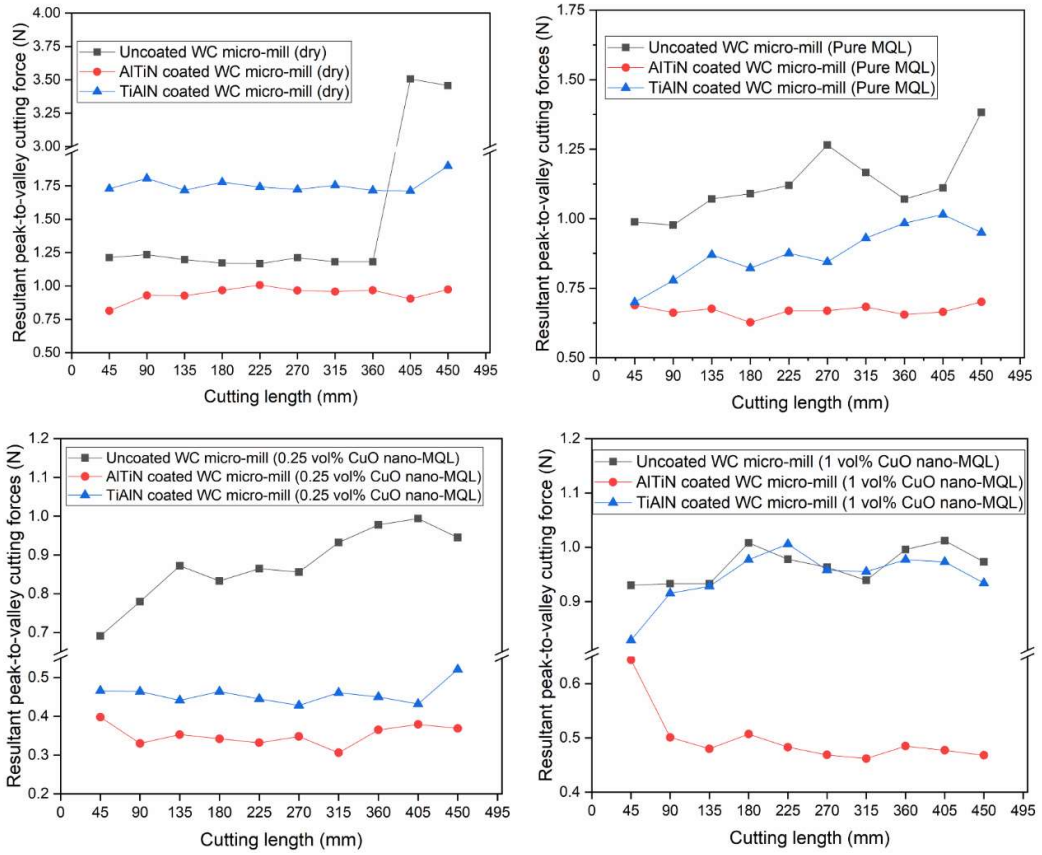

Fig. 4.19 The variation of cutting forces with machining length under different environments

Cross-feed force reveals similar patterns in the opposite phase; thus, only feed force is chosen [31]. Dashed lines represent the spindle rotations. Because the tool in consideration is a two fluted milling cutter, two peaks are formed for the whole cycle of the tool. Furthermore, owing to the tool run-out phenomenon, the peaks created by distinct teeth are not similar in a few cases. Fig. 4.20 illustrates the cutting forces obtained in micromilling under dry, deionized water MQL, 0.25 vol% CuO nanofluid

MQL, and 1 vol% CuO nanofluid MQL conditions with uncoated and AlTiN coated WC micro-mills.

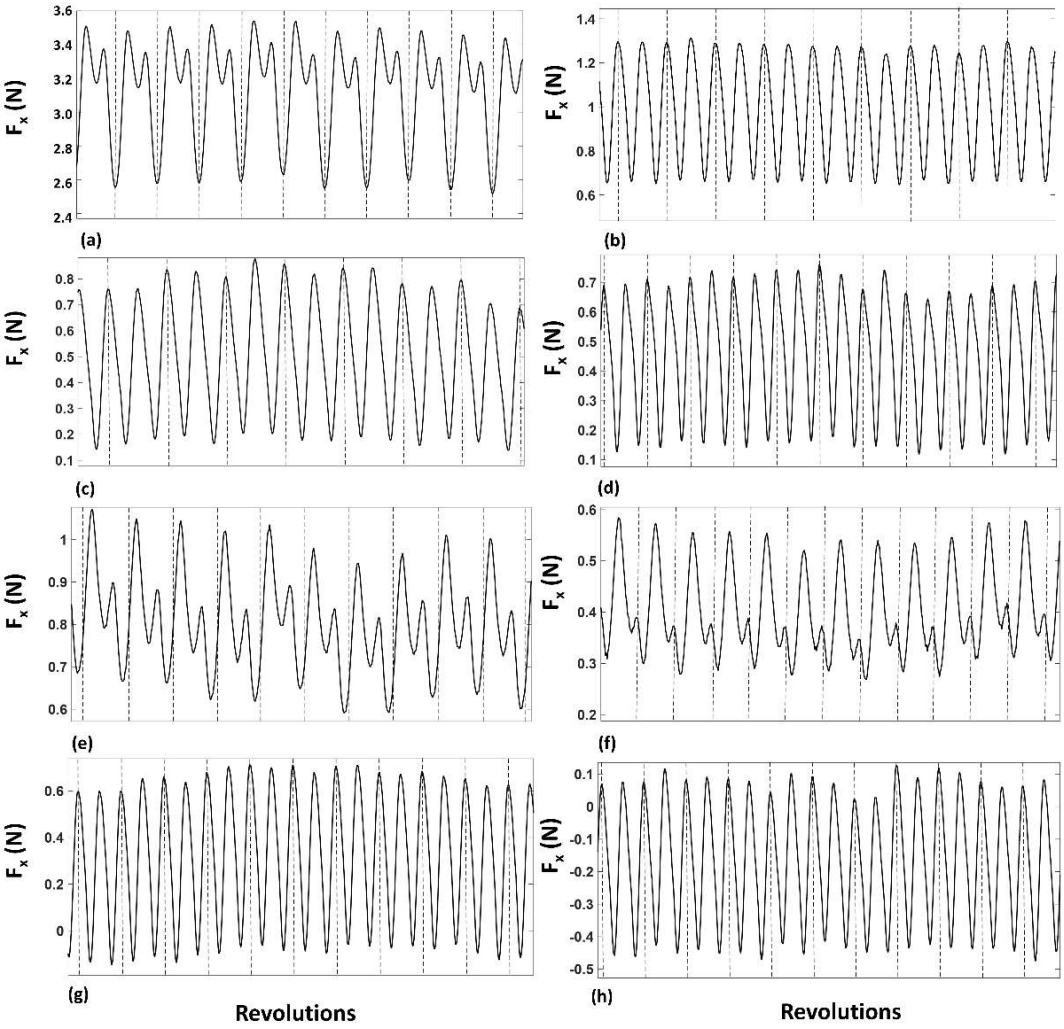

Fig. 4.20 Micromilling feed forces for uncoated and AlTiN coated WC tools: (a) & (b) for dry conditions, (c) & (d) for pure MQL (deionized water), (e) & (f) for 0.25 vol% CuO nanofluids MQL and, (g) & (h) for 1 vol% CuO nanofluids MQL conditions respectively

The cutting forces were significantly reduced using the AlTiN coated tool and nanofluid MQL condition, as illustrated in Figs. 4.20 (f) and (h). In dry conditions, the AlTiN coated WC tool shows lower cutting forces than the uncoated WC tool due to the low friction coefficient of the AlTiN coating film and the wear resistance of the hard AlTiN

coating layer. Sahoo et al. [100] found maximum cutting forces in the micromilling of P-20 steel using an uncoated tool. In contrast, the coated tools reduce cutting forces with a lower coefficient of friction. As observed in Fig. 4.20, the lower volume concentration of nanoparticles with the AlTiN coated tool yields lower cutting forces than other conditions. Due to nano ball-bearing effects, the spherical CuO nanoparticle's influence and confinement in the asperities of the surface reduce friction and are responsible for the significant reduction in cutting forces when using CuO nanofluids. Although at a higher concentration of nanoparticles, accumulation occurs, which collides with the pores on the workpiece surface, influencing surface roughness and generating higher cutting forces. A similar observation was carried out by Marcon et al. [15], where lower graphite concentrations contribute to lower tangential forces in the micromilling of AISI H13 tool steel.

4.2.3 Surface roughness

The smoothness of the machined surface is crucial in precision machining. To produce a quality product, it is necessary to investigate the surface roughness of the manufactured parts. Fig. 4.21 illustrates the surface roughness variations with machined length under different environments. Fig. 4.21 (a) shows the variation of average surface roughness (R_a) with cutting length in machining at dry conditions using uncoated and coated WC micro-mills. It can be observed that surface roughness (R_a) is significantly less for coated tools compared to uncoated ones. This can be attributed to the lower coefficient of friction and high wear resistance provided by the coating layer. From Fig. 4.21, it is observed that surface roughness first decreases and then increases with cutting length. In an uncoated WC micro-mill, surface roughness decreases up to 135 mm of machining length and increases afterward. In general, surface roughness decreases with an increase in edge radius value; however, after a specific edge radius

value, the size effect comes into play, and severe ploughing and rubbing occur. Due to the significant influence of ploughing and rubbing, surface roughness increases [31].

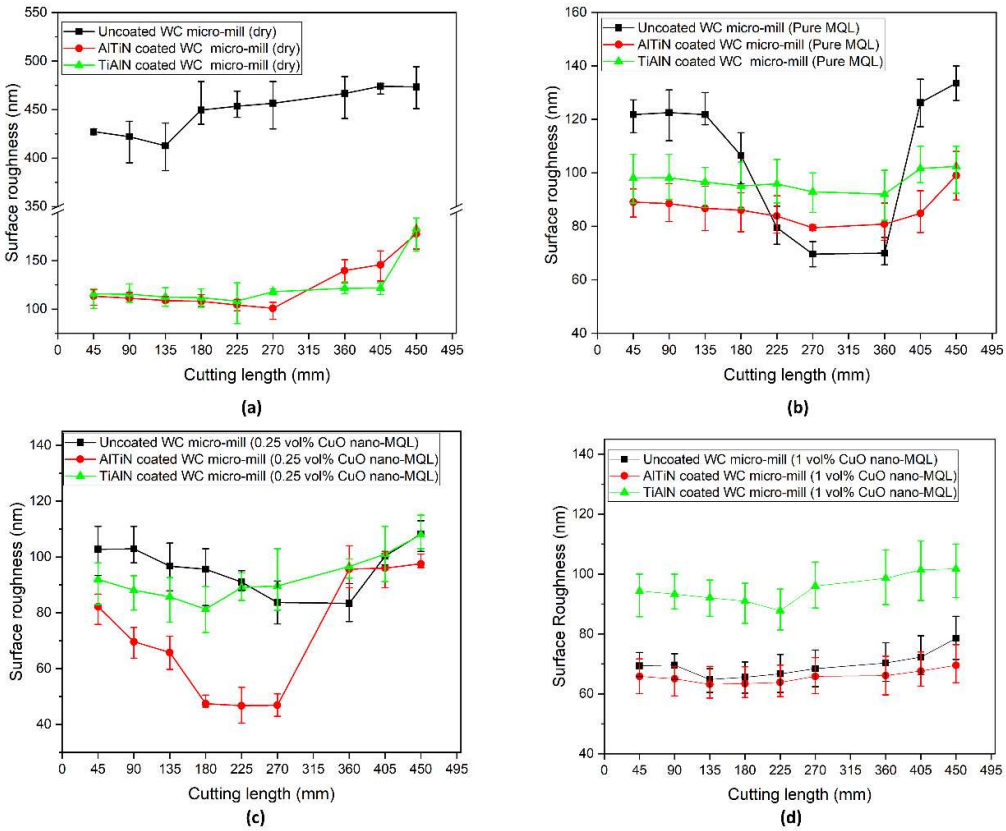

Fig. 4.21 The variation of average surface roughness with machining length by uncoated, AlTiN coated, and TiAlN coated WC micro end-mill in (a) dry (b) Pure MQL (c) 0.25 vol% CuO nanofluids MQL and (d) 1 vol% CuO nanofluids MQL conditions

Fig. 4.21 (b) shows the variation of average surface roughness with cutting length in pure MQL condition by uncoated, AlTiN coated, and TiAlN coated WC micro-mills. From Fig. 4.21 (b), the sudden enlargement of surface roughness after 360 mm machining length is found in the case of an uncoated WC micro end-mill. In contrast, coated WC tools show a very low variation of surface roughness with machining length. Among them, AlTiN coated tool offers better surface quality due to its low coefficient of friction and high hardness. Using a small amount of cutting fluid

and compressed air, MQL can create atomized droplets, lowering the cutting temperature during micromilling [112]. The lower tool adhesion due to MQL improves the surface finish of the microchannel than dry conditions. Pure MQL condition utilized deionized water, which possesses a high cooling capacity through convection and very low volatility. It protects tools from major edge chipping and significant adhesion that could affect the tool edge radius. Still, it has limited lubricating properties due to the lack of lubricating agents; therefore, it is insufficient to protect the coating from peeling off. Further, spherical CuO nanoparticles are added to deionized water to integrate the higher cooling rate of water with the lubrication capability of nanoparticles, and its effect on surface roughness has been analyzed.

Fig. 4.21 (c) illustrates the surface roughness variation with machining length in 0.25 vol% CuO NF-MQL using uncoated, AlTiN coated, and TiAlN coated WC micro end-mill. It is observed that AlTiN coating shows excellent results for surface quality. In some of the best cases, surface roughness was obtained lesser than 50 nm. With increasing cutting length, the surface roughness variations between the tools minimize, and roughness values at the end of the tenth slot are pretty close. Introducing nanofluids to the machining zone reduces heat-induced surface damage by reducing friction at the tool/chip and tool/workpiece contact and extracting heat faster due to the superior thermal conductivity of CuO nanoparticles [107]. Fig. 4.21 (d) illustrates the surface roughness variation with machining length in 1 vol% CuO NF-MQL condition using uncoated, AlTiN coated, and TiAlN coated WC micro end-mill. The variations of surface roughness in 1 vol% CuO NF-MQL are less significant than in other environmental conditions. It occurs due to the absence of adhesion and unworn cutting tool edges. Higher concentrations of nanoparticles improve wettability and maintain the sharpness of cutting edges. Because of their spherical shape, nanoparticles are subjected

to a ball-bearing effect between the sliding surfaces, converting sliding friction to rolling friction and lowering friction [113].

4.2.4 Burr formation and surface topography

Burr is considered an undesirable protrusion of materials due to plastic flow caused by cutting, shearing, and ploughing operations. Burrs are mainly classified as Poisson, rollover, tear, and cut-off burrs. Compared to conventional machining, burrs in micromilling cannot be ignored because burr size in micromilling is possibly comparable to or even more extensive than the depth of micro slots. Mostly large wavy top burrs are to be removed because it affects the performance of the components during assembly or fitting operation. Hence, micro burr morphology is the critical factor during the evaluation of surface accuracy of finished micro-features. Fig. 4.22 illustrates the SEM image of the microchannel made in dry condition using an uncoated WC micro end-mill, which shows down milling burr width is more than the up milling burr width. Fig. 4.23 shows the average top burr width of the 10th micro-slot in the down milling and up milling regions under different cutting environments. Fig. 4.23 illustrates the magnitude of down milling burr width is more extensive than the up milling burr width. In complete immersion milling, chip thickness varies from zero to feed per tooth in up milling, and then it goes from feed per tooth to zero in down milling. Chip thickness variation caused more deformed materials to accumulate towards the down milling side, which resulted in a larger burr size. In micromilling, the formation of burrs was greatly affected by tool wear. An uncoated tool in dry condition shows the maximum burr width due to maximum tool diameter reduction and edge chipping. Burr growth is caused by increased tool wear and ploughing dominated cutting operation in an uncoated WC tool under a dry state.

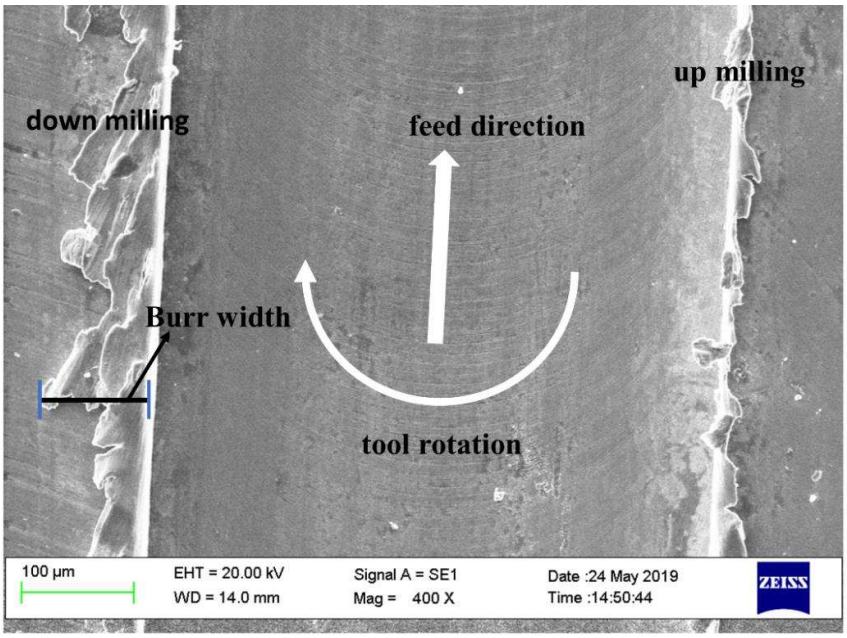

Fig. 4.22 Micro-channel made by the uncoated WC tool in dry condition showing the workpiece feed direction, down milling and up milling sides, and burr width measurement

Minimum average top burr widths of 9.93 µm and 10.58 µm were found in up milling and down milling, with AlTiN and TiAlN coated WC tools under 0.25 vol% CuO NF-MQL. Edge rounding of TiAlN coated tool in 1 vol% CuO NF-MQL caused the larger top burr width to form during up milling side. Fig. 4.24 shows the SEM images of micro-slots at the fragment of the cutting range of 405–450 mm, obtained under different cutting environments and coated tools. Fig. 4.24 (a) depicts the down-milling region produced more burr than the up-milling region by the uncoated WC micro end-mill in dry condition. A similar observation has been made from Fig. 4.24 (l); it occurred due to more consumption of specific energy on the down-milling side and a higher percentage of diameter reduction with edge chipping.

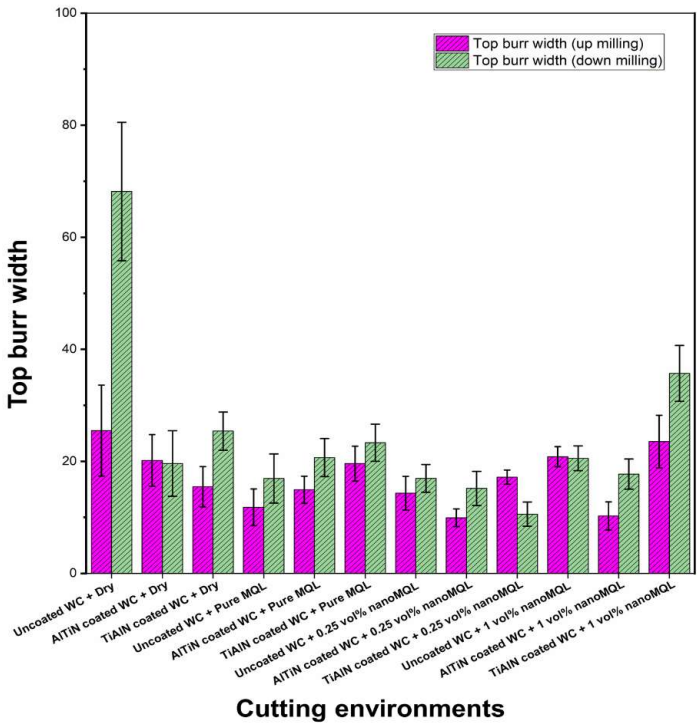

Fig. 4.23 Top burr width in up and down milling with different cutting environments between machining lengths of 405 mm and 450 mm

Fig. 4.24 (j–l) illustrates the smearing of CuO nanoparticles on the microchannel surface in the case of high volume concentration (1 vol%). The reason may be attributed to the accumulation of nanoparticles that adversely affect surface roughness and the smearing of nanoparticles over the machined surface. Fig. 4.25 shows SEM images of microchannels obtained using uncoated WC tool in 1 vol% CuO NF-MQL cutting environment. SEM images and EDS analysis of bottom surface in microchannel shows the presence of CuO nanoparticles in agglomerated form which is deposited on surface during tribofilm formation and different lubrication mechanism. Fig. 4.26 shows the surface topography obtained using uncoated, AlTiN coated, and TiAlN coated WC micro-mills in dry and pure MQL conditions. Surface defects are feed marks, ploughing pits, material debris, and burning surfaces. Fig. 4.26 (a–c) illustrates

the smearing of chip particles or workpiece materials on the machined surface due to the low thermal conductivity of Ti-6Al-4V alloy and high heat generation in dry conditions.

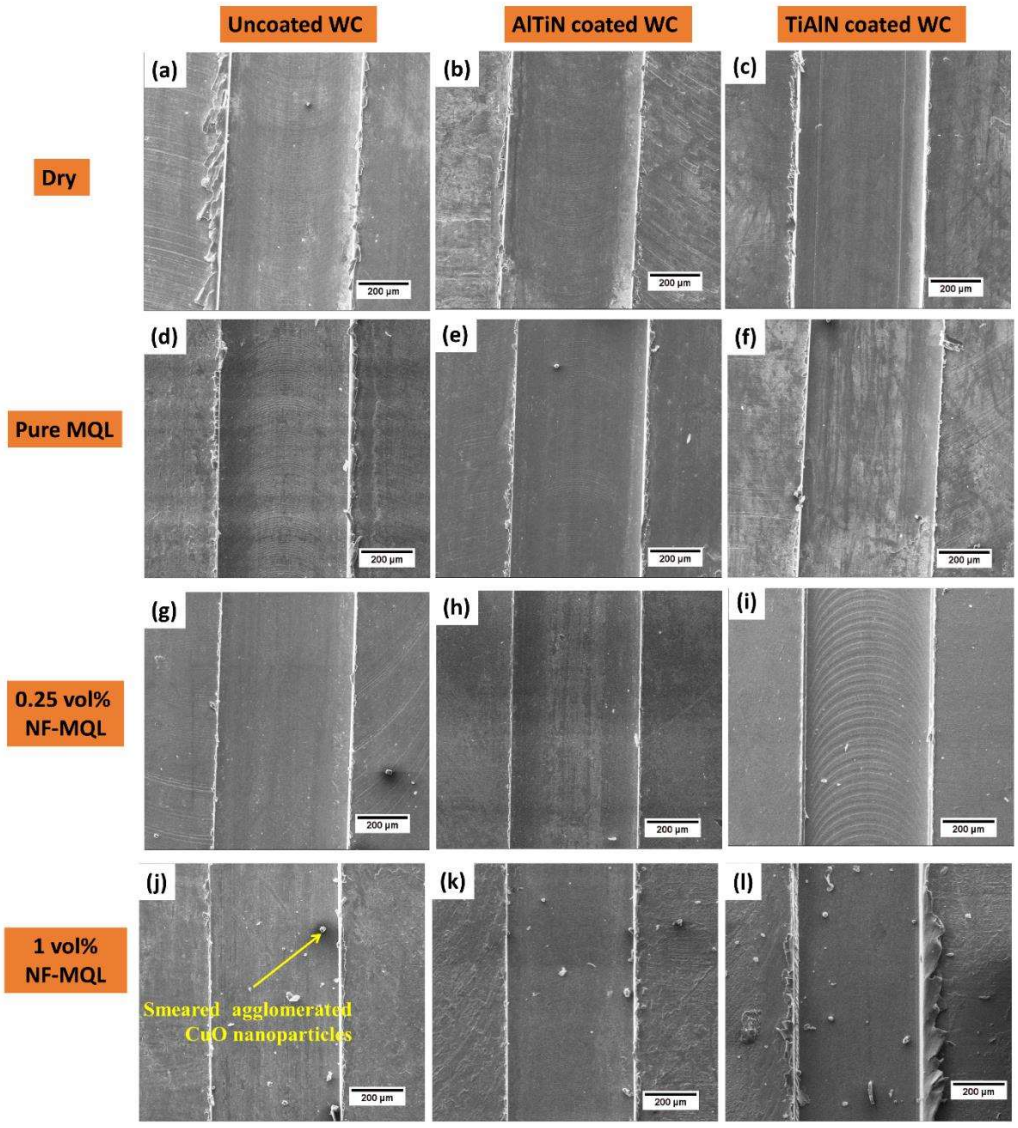

Fig. 4.24 The top view of SEM images of titanium alloy micro-slots was at the cutting distance between 405 mm and 450 mm for uncoated, AlTiN coated, and TiAlN coated WC micro-mills in dry condition, Pure MQL, CuO NF-MQL conditions with 0.25 vol% and 1 vol%

This resulted in built-up edge on cutting edges, which further deposited on the machined surface as smearing of the work materials. Chip adhesion on the milling cutter diminishes the chip removal capabilities of the tool significantly. As a result of the high friction and stress in the path parallel to the surface, plastic deformation arises on the workpiece surface in contact with the tool.

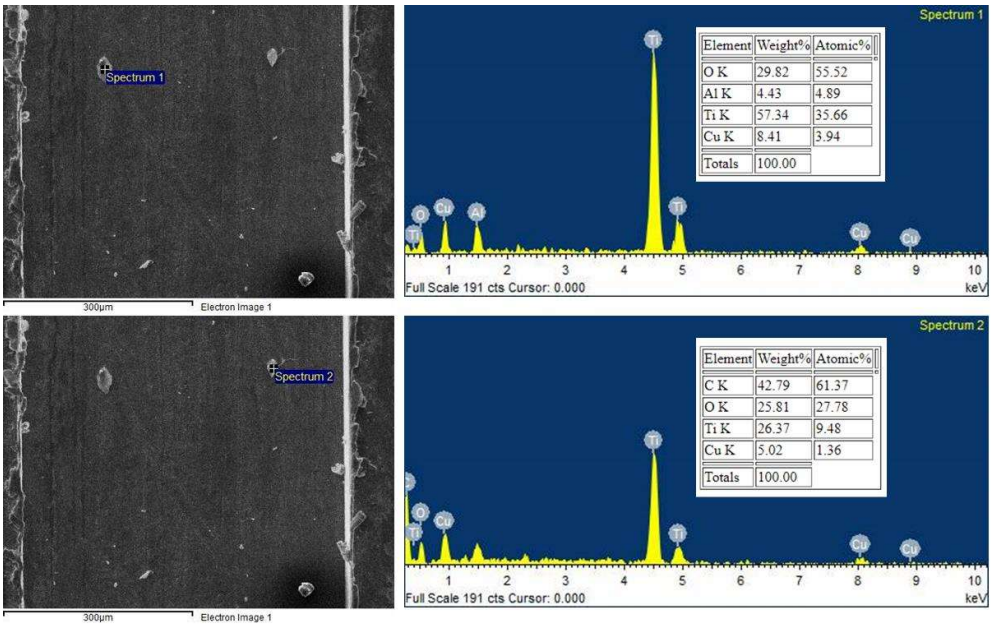

Fig. 4.25 SEM images and EDS analysis of machined surfaces lubricated with 1 vol% CuO nanofluids

A similar situation was obtained by Ucun et al. [114] in the micromilling of Inconel alloy; severe chip adhering on the machined surface occurs during dry cutting due to built-up edge formation. However, in MQL, the adhesion of work material on tools and chips smearing to the machined surface is less. In dry conditions, shearing is significant at first with a 4 µm/tooth feed, but the tooltips wear out, increase the cutting-edge radius, and the milling action shifts from shearing to ploughing at later cutting phases. Hence, workpiece material stuck to cutting edges in the form of a built-up edge instead of proper chip formation, further deposited to the bottom of the machined

surface. Fig. 4.26 (c) depicts nonuniform feed marks and chip adhesion on machined surfaces owing to both cutting edges of TiAlN coated tool being chipped. Fig. 4.26 (d–f) illustrates the smearing of chip or work-material is significantly less in pure MQL than in dry conditions due to better cooling of the cutting tool and lesser adhesion of the deformed chip towards cutting tools. The feed marks are more uniform, and the absence of plastic deformations was found in pure MQL.

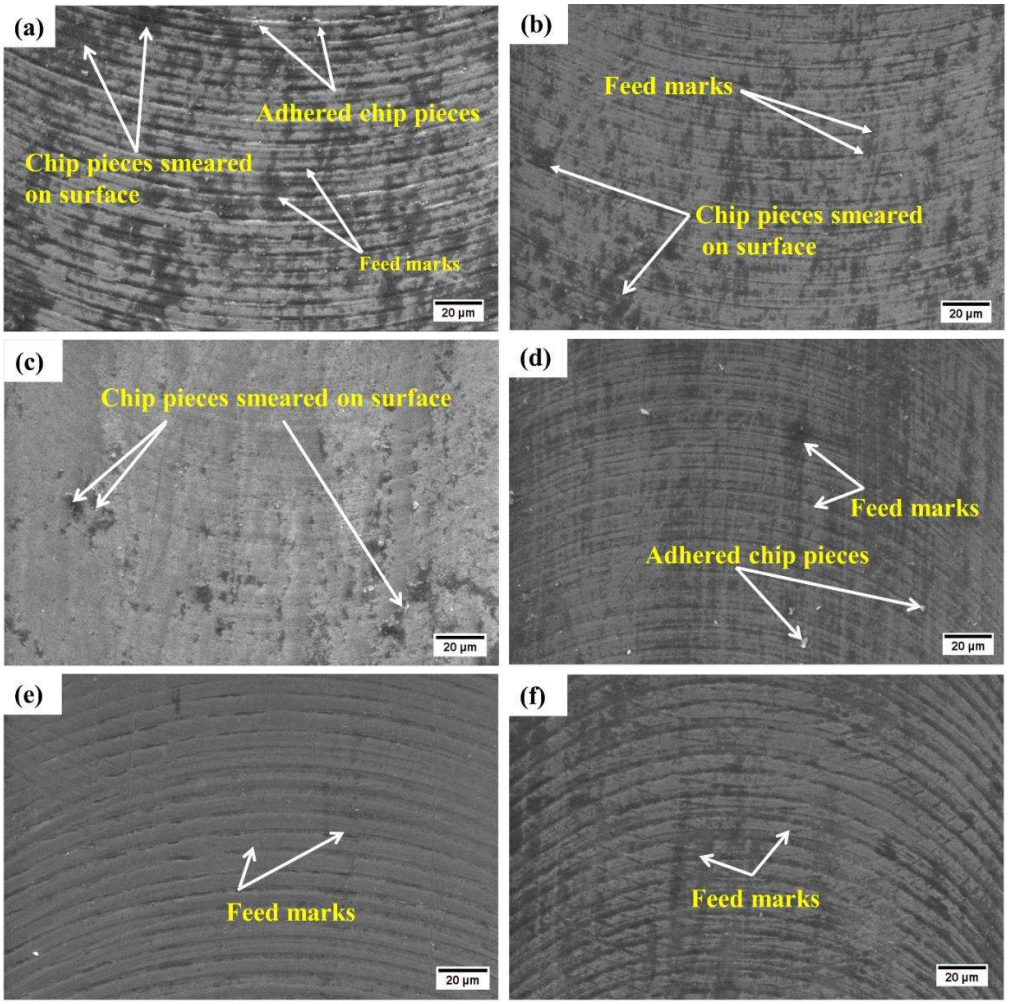

Fig. 4.26 Surface topography images of micro-milled surface produced by uncoated, AlTiN coated, and TiAlN coated WC micro-mills under (a)-(c) dry condition and (d)-(f) Pure MQL condition.

4.3 Summary

In this chapter, the influence of different cutting environments, including hybrid cutting environments (Dry, Pure MQL, 0.25 vol% CuO and 1 vol% CuO nanofluids MQL) along with different PVD coated (AlTiN coated and TiAlN coated) and uncoated WC micro end-mills were examined during micro-milling of Ti-6Al-4V alloy. The characteristics of CuO nanofluids, such as spherical size, dynamic viscosity, particle size in solution, XRD, and wettability over different cutting tools, were investigated. After analysis of the results, the findings could be summed up as following:

- Contact angles of CuO nanofluids on uncoated, TiAlN coated, and AlTiN coated WC substrate decrease with an increase in % volume concentration of CuO nanoparticles. It means that wettability improves with increasing volume concentration of nanofluids. Dynamic viscosity also increases with % volume concentration and an increase of 16.85% at 1 vol% CuO nanofluids observed than base fluid. In addition, the SEM micrograph shows that CuO nanoparticles are spherical, which is responsible for the improvement of the lubrication capability of nanofluids through ball-bearing effect. Furthermore, coated tools possess a low coefficient of friction had better wettability than uncoated tool. It is also observed that wettability is enhanced with an increase in the volume concentration of nanoparticles.
- According to tool wear analysis, a percentage of diameter reduction by 3.23% and absence of built-up-edge formation was observed in the uncoated WC micro end-mill under 1 vol% CuO NF-MQL due to high heat dissipation from the machining zone at high concentrations of CuO nanofluids.
- The burr width was measured for down and up milling in each cutting environment, and it was found that the AlTiN coated tool with 0.25 vol% CuO

NF-MQL proved to be more effective, resulting in burr widths that were reduced by 61.04% and 77.75% against dry conditions in up milling and down milling, respectively. Similarly, TiAlN coated tool reduced burr width by 36.52% and 82.53% in up and down milling, respectively. It can be related to the combined influence of the antifriction capabilities of spherical CuO nanoparticles and hard wear-resistant coated tools.

- Surface roughness was reduced by using AlTiN coated WC micro-mill with various cutting environments, and lower surface roughness values were obtained even lower than 50 nm under 0.25 vol% CuO NF-MQL cutting environment. The reason can be attributed to better lubrication properties in terms of the low coefficient of friction of CuO nanofluids and the high hardness of AlTiN coating.
- Using uncoated and coated tools, MQL generated a consistent surface topography with fewer defects.